Semiconducting Conjugated Coordination Polymer with High Charge Mobility Enabled by “4 + 2” Phenyl Ligands

Huang, X.; Fu, S.; Lin, C.; Lu, Y.; Wang, M.; Zhang, P.; Huang, C.; Li, Z.; Liao, Z.; Zou, Y.; Li, J.; Zhou, S.; Helm, M.; Petkov, P. S.; Heine, T.; Bonn, M.; Wang, H. I.; Feng, X.; Dong, R.;

Originally published:

January 2023

Journal of the American Chemical Society 145(2023), 2430-2438

DOI: https://doi.org/10.1021/jacs.2c11511

A Semiconducting Conjugated Coordination Polymer with High Charge Mobility Enabled by "4+2" Phenyl Ligands

Xing Huang[1, †], Shuai Fu[2, †], Jian Li[3], Yang Lu[1], Mingchao Wang[1], Peng Zhang[1], Chuanhui Huang[1], Zichao Li[4], Zhongquan Liao[5], Ye Zou[6], Chong Lin[7], Shengqiang Zhou[4], Petko St. Petkov[8], Thomas Heine[1], Mischa Bonn[2], Hai I. Wang[2*], Xinliang Feng[1,9*], Renhao Dong[1*]

[1] Center for Advancing Electronics Dresden (cfaed), Faculty of Chemistry and Food Chemistry, Technische Universität Dresden, Dresden 01062, Germany

[2] Max Planck Institute for Polymer Research, Mainz 55128, Germany

[3] Department of Fibre and Polymer Technology, KTH Royal Institute of Technology, Stockholm 10044, Sweden

[4] Institute of Ion Beam Physics and Materials Research, Helmholtz-Zentrum Dresden-Rossendorf, Dresden 01328, Germany

[5] Fraunhofer Institute for Ceramic Technologies and Systems (IKTS), Dresden 01109, Germany

[6] Institute of Chemistry Chinese Academy of Science, Beijing 100190 , China

[7] Department of Mechanical Engineering, The Hong Kong Polytechnic University, Kowloon, Hong Kong, China

[8] Faculty of Chemistry and Pharmacy, University of Sofia, Sofia 1164, Bulgaria

[9] Max Planck Institute of Microstructure Physics, Halle(Saale) 06120, Germany

[†]These authors contributed equally to this work

Email: wanghai@mpip-mainz.mpg.de; xinliang.feng@tu-dresden.de; renhao.dong@tu-dresden.de

Abstract

Electrically conductive coordination polymers are emerging as attractive electroactive materials for (opto-)electronics. However, developing semiconducting coordination polymers with high charge carrier mobility for logic devices has remained a great challenge so far, which urgently requires the rational design of ligands and topological networks as well as electronic structures. Herein, we demonstrate a strategy for the synthesis of high-mobility semiconducting conjugated coordination polymers (c-CPs) utilizing a new type of conjugated ligands, i.e., "4+2" phenyl ligands with D_{2h} symmetry. Compared with the traditional phenyl ligands with C_{6h} symmetry, the reduced symmetry

of the "4+2" ligands hinders the in-plane isotropic growth during the coordination reaction. Consequently, we successfully achieve a single-crystal three-dimensional (3D) c-CP Cu_4DHTTB (DHTTB = 2,5-dihydroxy-1,3,4,6-tetrathiolbenzene), which contains orthogonal ribbon-like *π-d* conjugated chains rather than 2D conjugated layers. The resulting Cu_4DHTTB exhibits a small bandgap (~0.2 eV), highly dispersed energy bands near the Femi level, and a small effective mass (~0.2 m*). Furthermore, it behaves as a p-type semiconductor with a room temperature conductivity of 0.2 S/cm, as disclosed by the four-probe method. Ultrafast terahertz spectroscopy confirms its semiconducting nature and demonstrates Drude-type transport of delocalized free carriers with high charge carrier mobility up to 88 ± 15 $cm^2 V^{-1} s^{-1}$, superior to thus-far reported conductive 3D coordination polymers. This work develops a molecular design strategy for constructing high-mobility semiconducting c-CPs, laying the foundation for achieving high-performance c-CPs-based (opto-)electronics.

Contents

Materials

All chemicals were purchased from Sigma-Aldrich and were used without future purification. Water has been degassed by the Freeze-Thaw method before being used.

Synthesis methods.

1. Synthesis of 2,5-dihydroxy-1,3,4,6-tetrathiolbenzene (DHTTB)

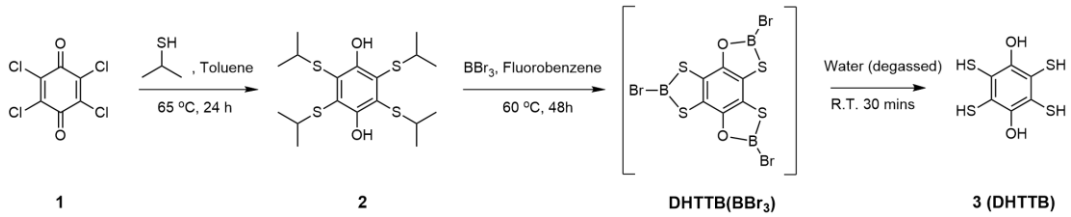

Scheme S1. Synthetic route of 2,5-dihydroxy-1,3,4,6-tetrathiolbenzene (**DHTTB**).

2,3,5,6-tetrakis(isopropylthio)benzene-1,4-dihydroquinone (**2**)

2,3,5,6-tetrakis(isopropylthio)benzene-1,4-dihydroquinone **2** was synthesized using a modified method based on literature[R]. Well-grounded sodium hydroxide (10g, 250 mmol) and 2-propanethiol (22.85 g, 300 mmol, 28.21 mL) were added into toluene and stirred for 3 hours at ambient temperature to make a well-dispersed suspension. Then, dropwise, 300 ml of toluene solution containing p-chloranil (12.94 g, 50 mmol) was added and reacted at 65 °C for 24 hours. After the reaction mixture was cooled to ambient temperature, 200 mL of Mili-Q water was added to the mixture. After heavily stirring the mixture for 1 hour, the organic layer was separated and dried over anhydrous magnesium sulfate. The solvent was removed by rotary evaporation and recrystallization of residue from hot methanol (150 mL) giving **2** as white needle crystals.

2,5-dihydroxy-1,3,4,6-tetrathiolbenzene (**3**)

2,3,5,6-tetrakis(isopropylthio)benzene-1,4-dihydroquinone **2** was dissolved in dried fluorobenzene to form a colorless solution. BBr_3 was added dropwise into the solution, and the mixture was heated to 60 °C for 48 hours and then cooled down to room temperature. After the solution cooled, a white precipitate formed. The white precipitate was filtered out and washed with dry fluorobenzene. This product is the borylations derivate of DHTTB (denoted as DHTTB(BBr_3)). However, due to the sensitivity of B-Br bond in the DHTTB(BBr_3) , it was used directly for the next reaction without further treatment. DHTTB(BBr_3) was transferred into a flask under nitrogen, and degassed water was added. After reaction for 1 hour under stirring, the resultant white precipitate was collected by suction filtration, washed with cold water, and dried under vacuum to yield DHTTTB. 1H NMR (500 MHz, Toluene-d6): δ = 5.80 (2H), 3.27 (4H) ppm(Figure S12). Elemental analysis (calcd., found for: C (30.24, 30.94), H

(2.54, 2.43), S (53.80, 53.74). Mass spectrometry analysis (DHTTB = M, calc. [M+H]+ = 239.0000 found 239.0000).

2. Synthesis of Cu_4DHTTB

Under nitrogen, degassed water was added into a 20 mL glass vial containing DHTTB and $CuSO_4 \cdot 5H_2O$. Then the mixture was stirred and heated to 80 °C. After the reaction at 80 °C for 12 hours, the solid products were filtrated from the solution and washed with dimethyl formamide, acetonitrile, and menthol. Then it was dried under a dynamic vacuum for 24 h. Yield of black powder of Cu_4DHTTB: 0.135 g, 91%. Anal. Calcd for $Cu_4C_6S_4O_2$: Cu, 52.25; C, 14.81. Found: Cu, 51.74; C, 14.71.

Based on a literature-reported method[1], film samples of Cu_4DHTTB and Cu_3BHT were synthesized by the same interfacial reaction method. More specifically, $CuSO_4$ was dissolved in 30 mL of water and added to a beaker. The aqueous solution was carefully covered by 30 mL of toluene which served as a buffer layer. 1 mL of a toluene solution of the ligand (20 μM) was slowly injected into the organic upper phase. Film samples will form and can be observed after the reaction last for several minutes. Then the samples were transformed onto the quartz substrate and rinsed with DMF, acetonitrile, methanol, and acetone. Finally, the film sample was dry under a vacuum at 80 °C for further use.

Characterization methods

Component characterization and analysis

Copper contents have been measured by using inductively coupled plasma optical emission spectrometry (ICP-OES, iCAP 6300 Radial, Thermo Scientific) . Carbon and sulfur content analysis has been performed by using CHN elemental analysis (Flash EA 1112, Thermo Fisher Scientific).

Powder x-ray Diffraction (PXRD)

The PXRD data were collected by using Aries (Panalytical) equipped with Cu Kα radiation (λ = 1.5404 A).

3D Electron Diffraction Technique, continuous Rotation Electron Diffraction (cRED)

Three-dimensional electron diffraction (3D ED) data were collected using the c-RED method implemented in the software Instamatic. All the datasets were collected using a JEOL JEM2100 TEM (LaB6 filament, ASI Timepix camera) operating at 200 kV. The reciprocal space reconstruction was carried out using the program RED, and the reflection intensity extraction was conducted by the program

XDS. Using the intensities obtained from 3D ED data, the structures were solved ab initio by the software package SHELXT 9.

Raman spectroscopic characterization

Raman spectra have been recorded using a Horiba LabRAM HR Evolution Raman microscope in the range of 120–4000 cm^{-1} at 298 K. The resolution for all measurements was 4 cm^{-1} and 256 scans. The Raman spectra of Cu_4DHTTB and DHTTB can be found in Figure S1. DHTTB featured strong signals at ~2550 cm^{-1} and 3350 cm^{-1} that can be ascribed to the S−H stretching vibration and O-H stretching vibration, respectively[2]. Both those peaks disappeared completely in Cu_4DHTTB.

Scanning Electron Microscopy (SEM)

The Scan Electrical Microscope (SEM) images were obtained by a Toshiba S4800 SEM. The High-Resolution Transmission Electron Microscopy (HRTEM) images were obtained by using a JEOL 2100F TEM with an accelerated voltage of 120 kV.

Electrical property measurement

To measure the electrical property of Cu4DHTTB, Cu4DHTTB crystals were pressed into pellet samples under 500 MPa of pressure. And then, four parallel gold electrodes were deposited on them through low-temperature vacuum evaporation to form a four electrode setup. The electrical conductivity was measured in a Lake Shore Hall system. The current used for resistivity measurement is 100 mA.

Ultrafast THz spectroscopy

Ultrafast THz spectroscopy was used to investigate the charge transport properties of Cu_3BHT and Cu_4DHTTB films deposited on fused silica substrates. The setup employs a commercial Ti:sapphire laser amplifier system to generate ultrafast laser pulses with a central wavelength of 800 nm, a duration of ~50 fs, and a repetition rate of 1 kHz for optical excitation, THz generation and detection. By using a pair of (110) ZnTe crystals, single-cycle THz pulses of ~1 ps duration were generated and detected by optical rectification and free-space electro-optic sampling, respectively. For characterizing the intrinsic electrical properties, THz waveforms transmitted through a blank SiO_2 substrate and Cu_3BHT and Cu_4DHTTB films deposited on the substrates were recorded in the absence of photoexcitation. By Fourier transform the time-domain THz waveforms to the frequency domain, the frequency-resolved complex THz conductivity $\sigma(\omega)$ of Cu_3BHT and Cu_4DHTTB films can be obtained via equation (1):

$$\frac{E(w)}{E_0(w)} = \frac{n+1}{n+1+Z_0\sigma(w)} \quad (1)$$

where $E_0(w)$ is the frequency-dependent THz electrical field transmitted through the blank SiO_2 substrate, $E(w)$ is the frequency-dependent THz electrical field transmitted through Cu_3BHT or Cu_4DHTTB, Z_0 = 377 Ω is the impedance of free space, and n = 1.95 is the refractive index of the

used SiO_2 substrate in the THz range. The dynamics and transport properties of Cu_3BHT and Cu_4DHTTB films were characterized by optical-pump THz-probe (OPTP) spectroscopy, in which the THz transmission in the absence (E_{unpump}) and presence (E_{pump}) of photoexcitation were recorded in transmission mode. The complex THz photoconductivity ($\Delta\sigma(\omega)$) can be obtained via the thin-film approximation, as shown in equation (2):

$$\Delta\sigma(\omega) = -\frac{n_1 + n_2}{Z_0 l} \cdot \frac{\left(E_{pump}(\omega) - E_{\mathrm{unpump}}(\omega)\right)}{E_{\mathrm{unpump}}(\omega)} \quad (2)$$

The fluence-dependent measurements were performed in a dry N_2 environment, and the samples were photoexcited by the 800 nm laser pulses with pump fluences ranging from 29 to 79 μJ/cm^2. The temperature-dependent THz photoconductivity measurements were conducted under vacuum conditions (pressure < 2×10^{-4} mbar) with the help of a cryostat.

Calculation details

The electronic structures (HOMO, LUMO, and electrostatic potential (ESP)) and optimized structures of benzene-based conjugated ligands are derived from DFT calculations. DFT was performed using Gaussian 09 with the B3LYP functional and 6-311g(d,p) basis set and the Grimme D3 dispersion correction. (Gaussian 09, Revision C.01, M. J. Frisch, G. W. Trucks, H. B. Schlegel, G. E. Scuseria, M. A. Robb, J. R. Cheeseman, G. Scalmani, V. Barone, B. Mennucci, G. A. Petersson, H. Nakatsuji, M. Caricato, X. Li, H. P. Hratchian, A. F. Izmaylov, J. Bloino, G. Zheng, J. L. Sonnenberg, M. Hada, M. Ehara, K. Toyota, R. Fukuda, J. Hasegawa, M. Ishida, T. Nakajima, Y. Honda, O. Kitao, H. Nakai, T. Vreven, J. A. Montgomery Jr., J. E. Peralta, F. Ogliaro, M. Bearpark, J. J. Heyd, E. Brothers, K. N. Kudin, V. N. Staroverov, T. Keith, R. Kobayashi, J. Normand, K. Raghavachari, A. Rendell, J. C. Burant, S. S. Iyengar, J. Tomasi, M. Cossi, N. Rega, J. M. Millam, M. Klene, J. E. Knox, J. B. Cross, V. Bakken, C. Adamo, J. Jaramillo, R. Gomperts, R. E. Stratmann, O. Yazyev, A. J. Austin, R. Cammi, C. Pomelli, J. W. Ochterski, R. L. Martin, K. Morokuma, V. G. Zakrzewski, G. A. Voth, P. Salvador, J. J. Dannenberg, S. Dapprich, A. D. Daniels, O. Farkas, J. B. Foresman, J. V. Ortiz, J. Cioslowski, D. J. Fox, Gaussian, Inc., Wallingford CT, 2010.)

We investigated the electronic structures of Cu-DHTTB based on first-principles calculations in Vienna Ab initio Simulation Package (VASP) 5.3 code[3]. All calculations were performed employing Generalized Gradient Approximations (GGA)-PBE exchange-correlation functional with D2 dispersion correction[4, 5] and a Projector-Augmented Wave (PAW) potential[6]. Monkhorst-Pack scheme was selected to generate k meshes. And the plane-wave basis was set up to 600 eV cutoff. The optimized crystal structures that are good agreement with experimental parameters were obtained at a convergence threshold of ionic relaxation with 0.02 eV/ Å. Then band structures and Projected Density-of-States (PDOS) were performed at PBE level.

The points of high symmetry in the calculated Brillouin zone[7] are labeled as follows:

Γ= (0, 0, 0); Z= (0, 0.5, 0); D= (0, 0.5, 0.5); B= (0, 0, 0.5); A (-0.5, 0, 0.5); E (-0.5, 0.5, 0.5); Z (0, 0.5, 0.); C_2 (-0.5, 0.5, 0); Y_2 (-0.5, 0, 0)

The zero energy is given at the Fermi energy.

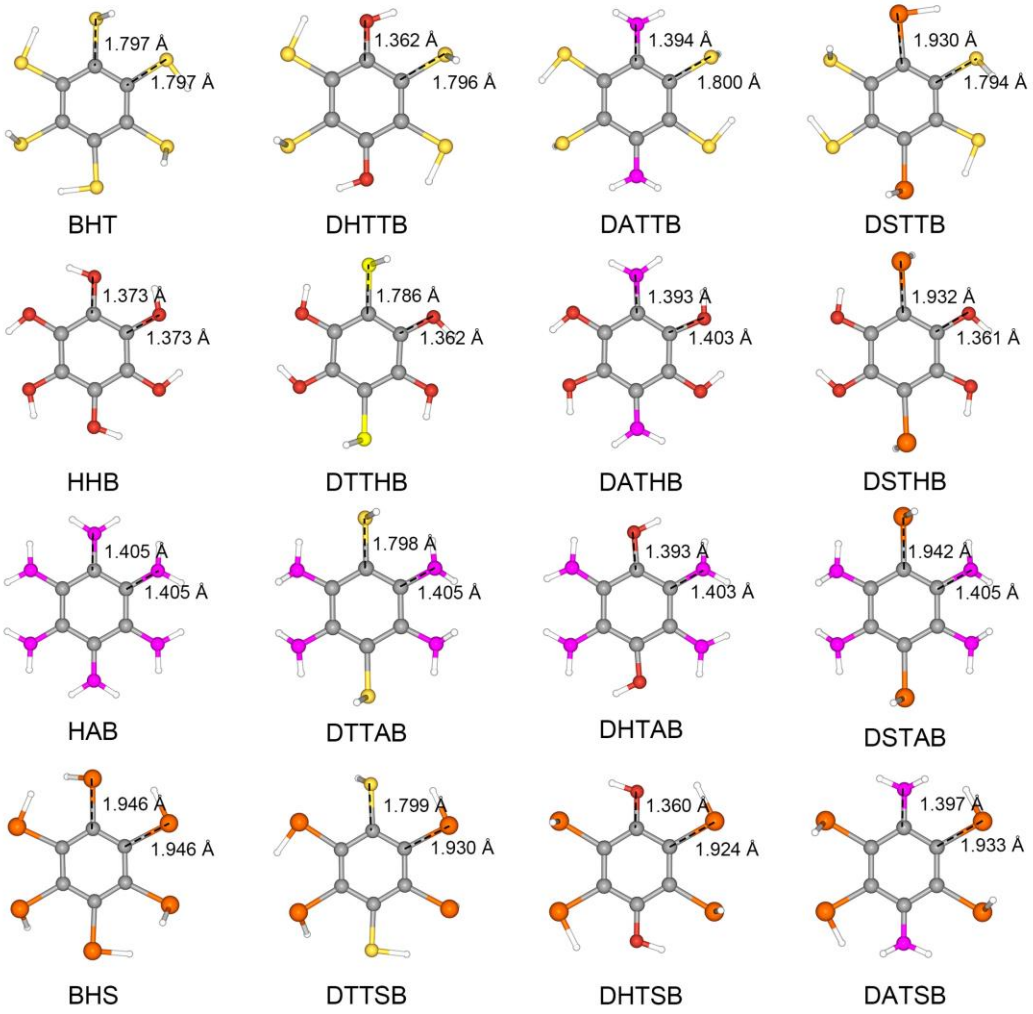

Figure S1. Calculated bond length information for benzene-based conjugated ligands including benzenehexathiol(**BHT**), 1,4-dihydro-2,3,5,6-tetrathiolbenzene(**DHTTB**), 3,6-diamino-1,2,4,5-tetrathiolbenzene(**DATTB**), 3,6-diselenol-1,2,4,5-tetrathiolbenzene(**DSTTB**), hexahydroxybenzene(**HHB**), 3,6-dithiol-1,2,4,5-tetrahydrobenzene(**DTTHB**), 3,6-diamino-1,2,4,5-tetrahydrobenzene(**DATHB**), diselenol-1,2,4,5-tetrahydrobenzene,(**DSTHB**) hexaaminobenzene(**HAB,**) 1,4-dithiol-2,3,5,6-tetraaminobenzene(**DTTAB**), 1,4-dihydrol-2,3,5,6-tetraaminobenzene(**DHTAB**), 1,4-diselenol-2,3,5,6-tetraaminobenzene(**DSTAB**), benzenehexaselenol(**BHS**), 3,6-dithiol-1,2,4,5-tetraselenolbenzene(**DTTSB**), 3,6-dihydro-1,2,4,5-tetraselenolbenzene(**DHTSB**) and 3,6-diamino-1,2,4,5-tetraselenolbenzene(**DATSB**).

.

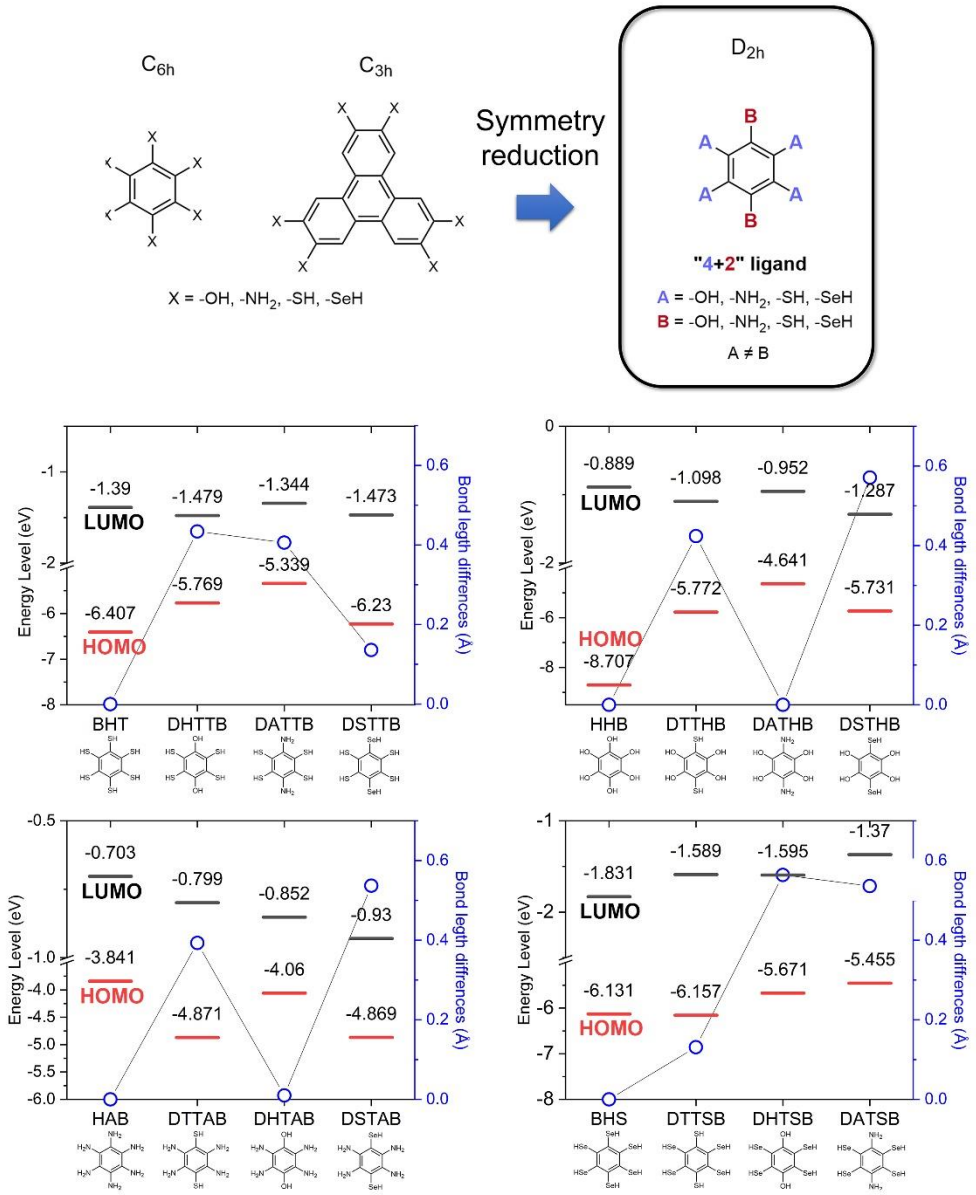

Figure S2. Calculated HOMO and LUMO energy levels and absolute bond length difference between different substitution groups(|D(C-A)-D(C-B)|) in "4+2" ligands.

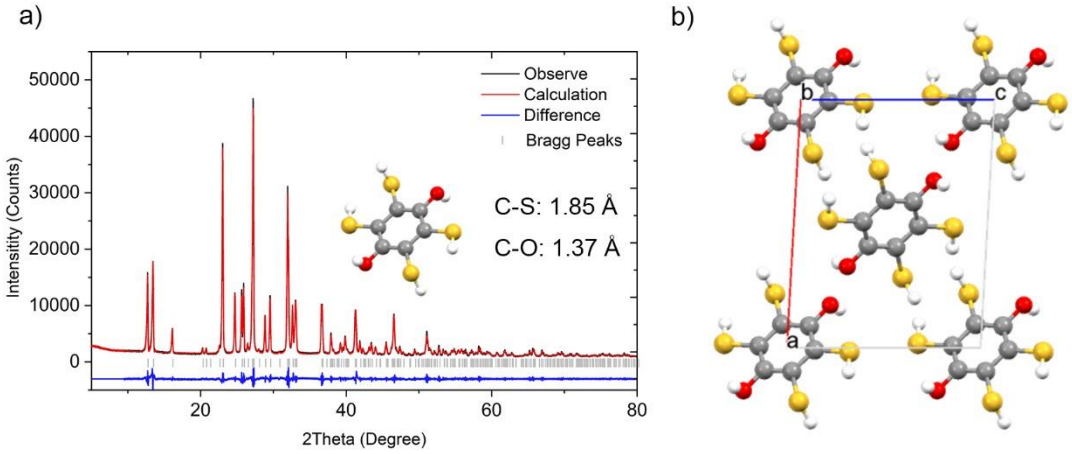

Figure S3. Powder refinement against Powder X-ray Diffraction (PXRD) of DHTTB and the as-solved crystal structure of DHTTB. (a) Rietveld refinement of the PXRD pattern of DHTTB. (b) Presentation of crystal structure of DHTTB along [010] direction.

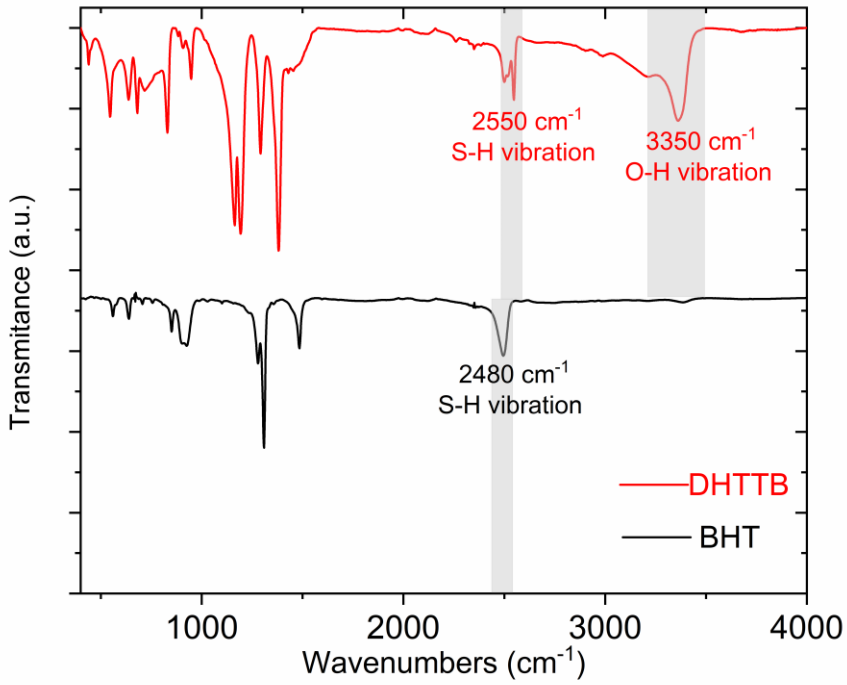

Figure S4. Fourier transform-infrared (FT-IR) spectra of BHT and DHTTB.

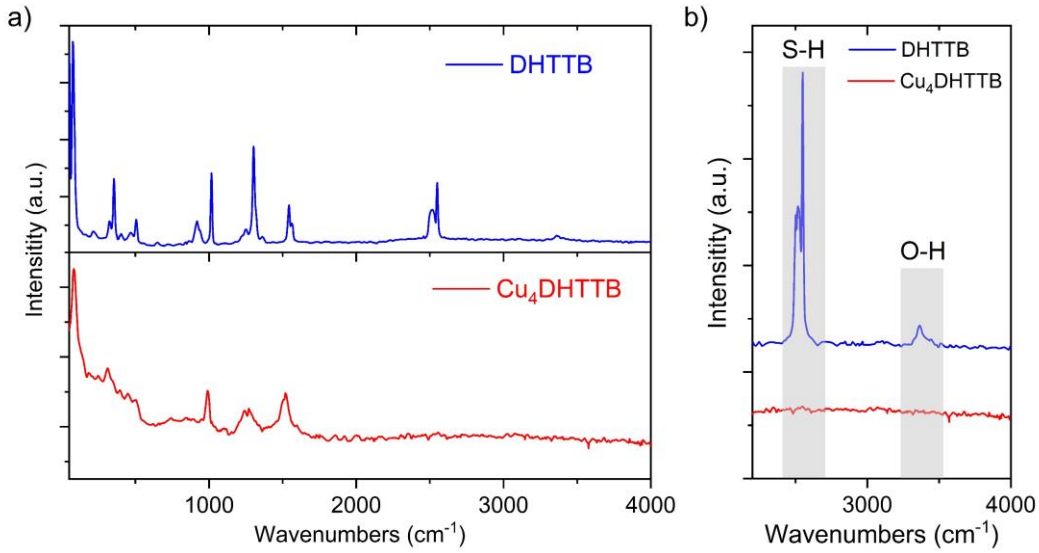

Figure S5. Raman Spectra of DHTTB and Cu_4DHTTB.

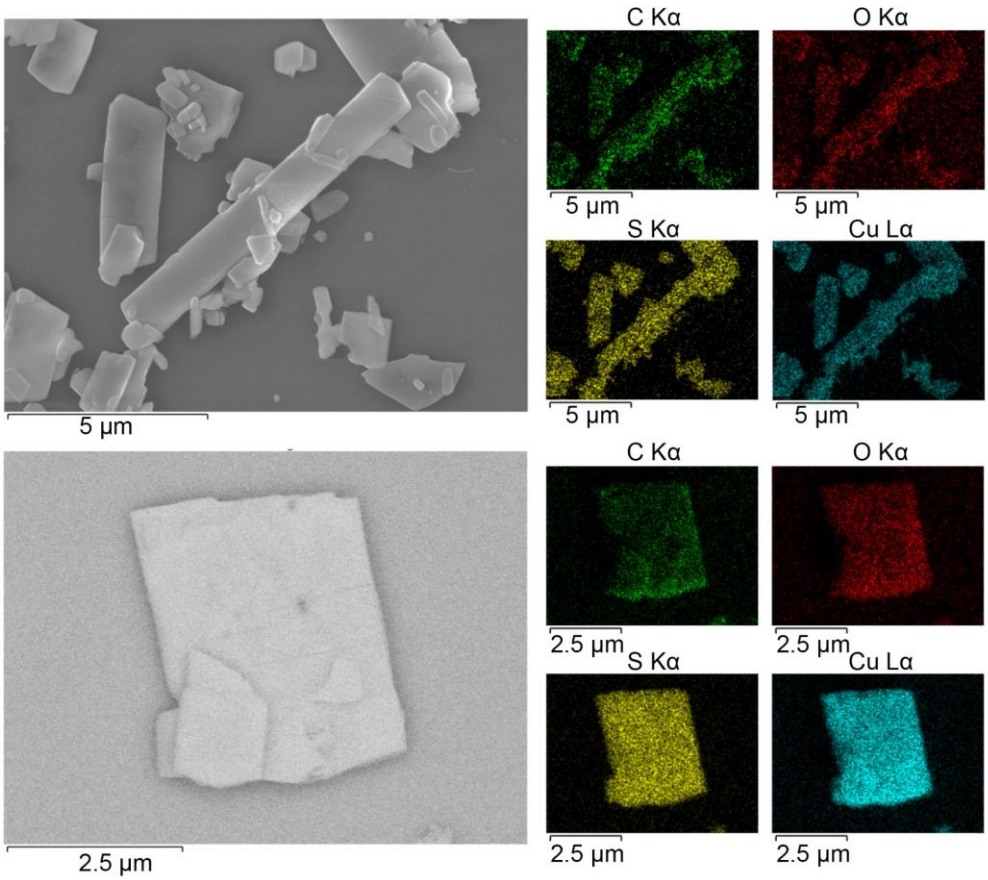

Figure S6. EDS elemental mapping images of Cu(cyan), S(yellow), C(green) and O(red) for crystal of Cu_4DHTTB.

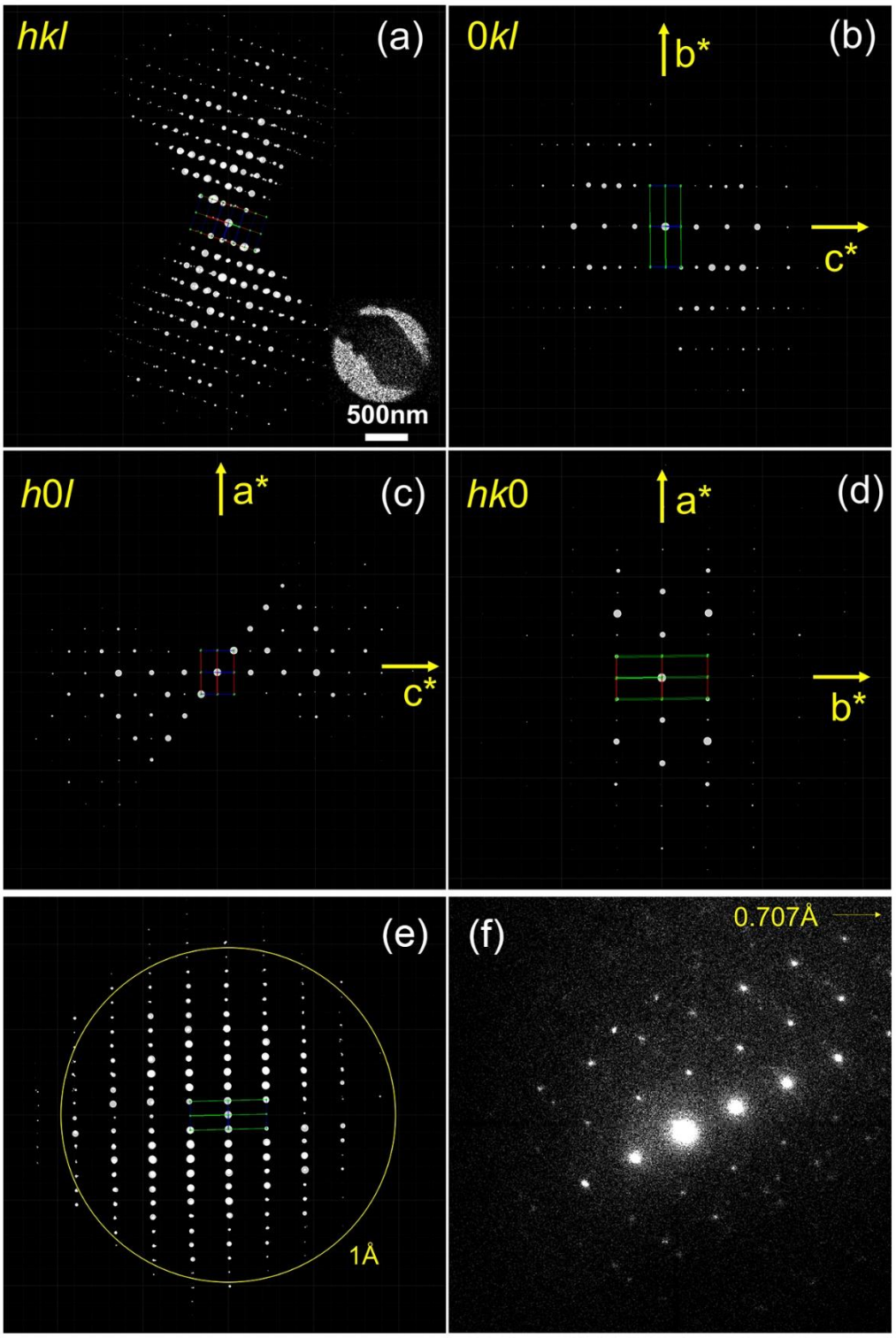

Figure S7. Electron diffraction data collected by continuous rotation electron diffraction (c-RED). a) Data overview and reconstructed reciprocal space alone a* axis (b), b* axis (c) and c* (axis). Slice of reconstructed reciprocal space (e) and (f) typical electron diffraction patterns which show high-resolution data up to 0.707 Å.

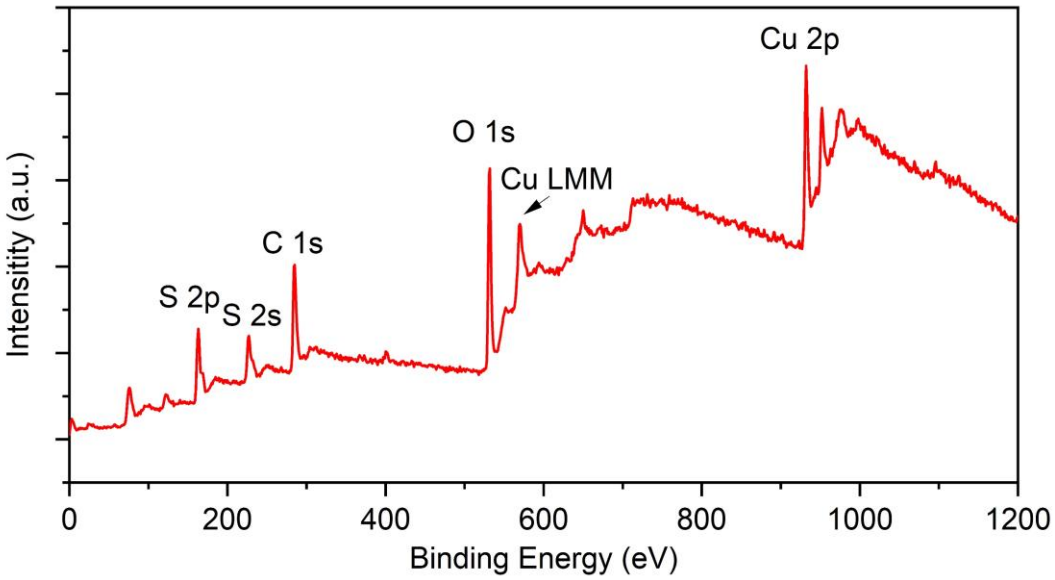

Figure S8. Full X-Ray Photoelectron Spectroscopy (XPS) spectrum of Cu_4DHTTB**.**

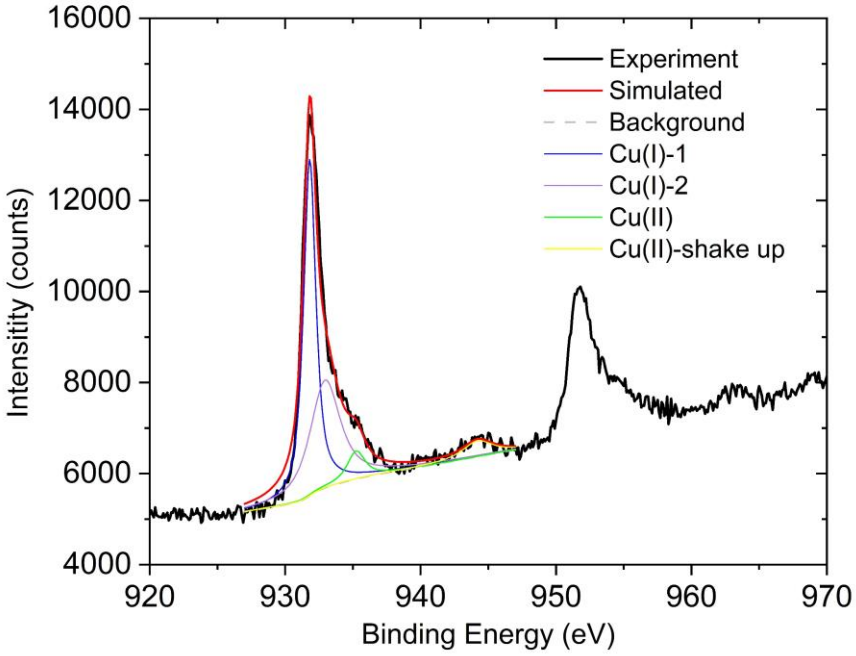

Figure S9. High-resolution XPS spectrum of Cu_4DHTTB focused on Cu 2p region.

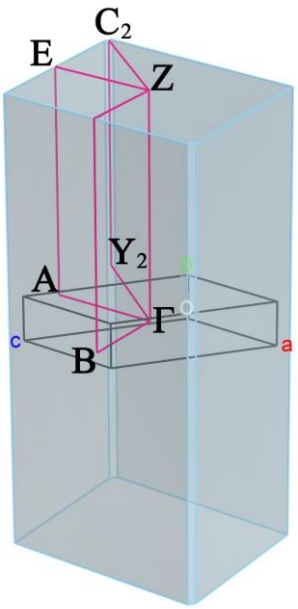

Figure S10. Illustration of the high-symmetry K-points in first Brillouin zone of Cu_4DHTTB

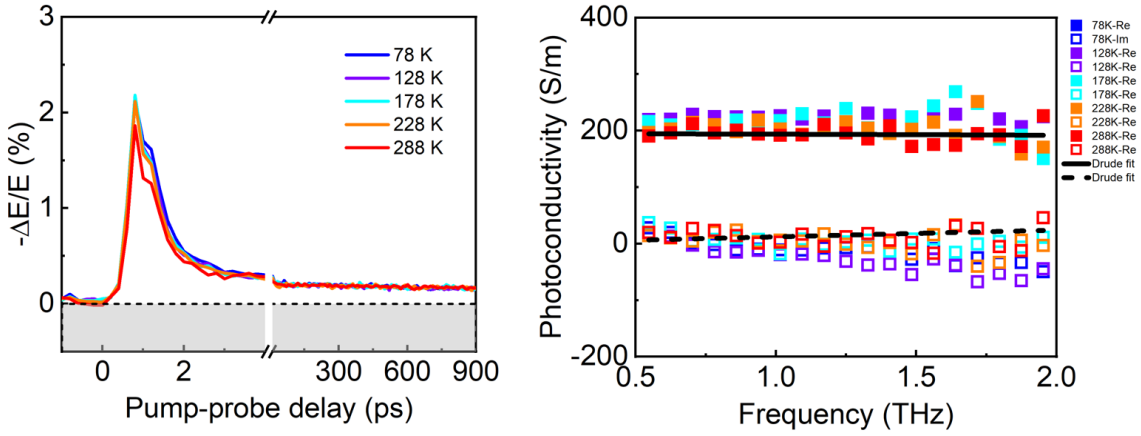

Figure S11. Temperature-dependent THz photoconductivity of Cu_4DHTTB. (a) Time-resolved THz photoconductivity of Cu_4DHTTB at different temperatures. (b) Frequency-resolved THz photoconductivity of Cu_4DHTTB at different temperatures.

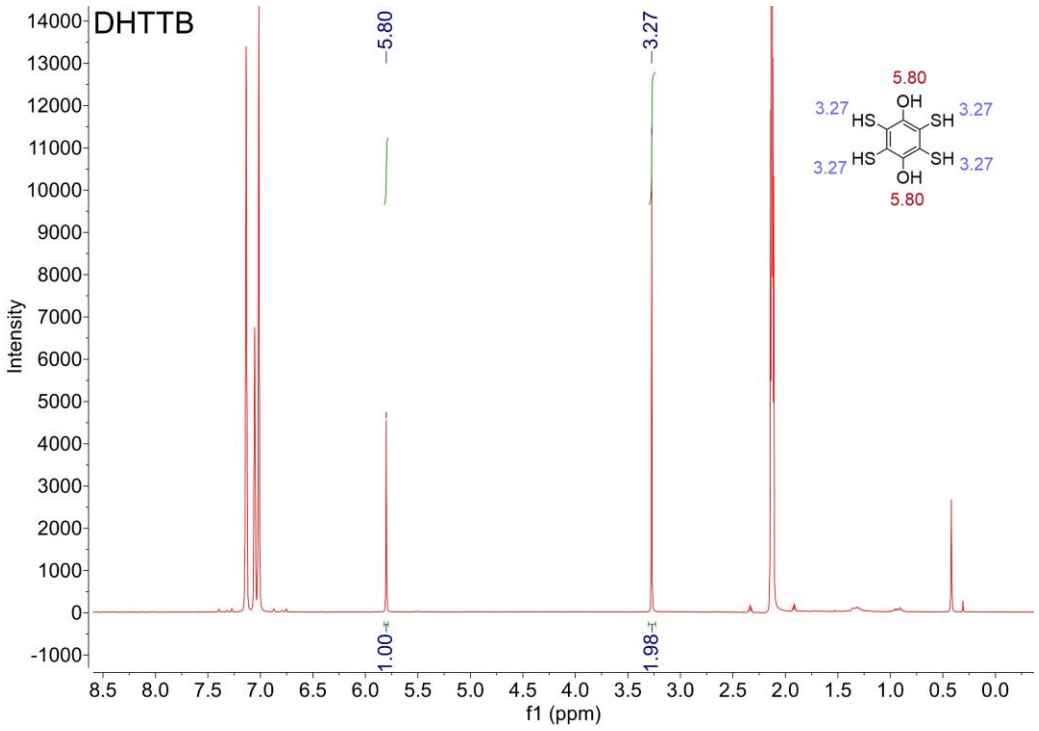

Figure S12. ^{1}H-NMR spectrum of DHTTB

Table S1. Summary of the charge mobility and corresponding measurement methods of 3D conductive MOFs/CPs.

Materials	Mobility	Mobility Mesurment techlogy	Ref
Cu_4DHTTB (DHTTB=2,5-dihydroxy-1,3,4,6-tetrathiolbenzene)	88 ± 15 $cm^2 V^{-1} s^{-1}$	THz mobility	This work
$K_{0.98}$ $Fe_2(BDP)_3$ (BDP2− = 1,4-benzenedipyrazolate)	0.84 $cm^2 V^{-1} s^{-1}$ (*e*)	Single crystal FET device mobility	[8]
$K_{0.98}$ $Fe_2(BDP)_3$	0.29 $cm^2 V^{-1} s^{-1}$	FP-TRMC mobility	[8]
$Fe_2(BDP)_3$	0.02 $cm^2 V^{-1} s^{-1}$	FP-TRMC mobility	[8]
Zn_2(TTFTB) (H_4TTFTB=tetrathiafulvalene-tetrabenzoate)	0.2 $cm^2 V^{-1} s^{-1}$	FR-TRMC mobility	[9]
Mn_2(DSBDC) (H_4DSBDC =2,5-disulfhydrylbenzene-1,4-dicarboxylic acid)	0.02 $cm^2 V^{-1} s^{-1}$	FR-TRMC mobility	[10]
$[In(isophthalate)_2]^-$	4.6×10^{-3} $cm^2 V^{-1} s^{-1}$	Drop-cast Film FET device mobility	[11]

FET(Field-effect transistor)

FP-TRMC(flash-photolysis-time-resolved microwave conductivity)

Reference

[1] Huang, X., *et al.* Superconductivity in a Copper(II)-Based Coordination Polymer with Perfect Kagome Structure. *Angew. Chem. Int. Ed. Engl.* **57**, 146-150 (2018).

[2] Kambe, T., *et al.* pi-Conjugated nickel bis(dithiolene) complex nanosheet. *J. Am. Chem. Soc.* **135**, 2462-2465 (2013).

[3] Kresse, G., Furthmüller, J. Efficiency of ab-initio total energy calculations for metals and semiconductors using a plane-wave basis set. *Comput. Mater. Sci.* **6**, 15-50 (1996).

[4] Perdew, J. P., Burke, K., Ernzerhof, M. Generalized Gradient Approximation Made Simple. *Phys. Rev. Lett.* **77**, 3865-3868 (1996).

[5] Grimme, S. Semiempirical GGA-type density functional constructed with a long-range dispersion correction. *J. Comput. Chem.* **27**, 1787-1799 (2006).

[6] Blöchl, P. E. Projector augmented-wave method. *Phys. Rev. B* **50**, 17953-17979 (1994).

[7] Setyawan, W., Curtarolo, S. High-throughput electronic band structure calculations: Challenges and tools. *Comput. Mater. Sci.* **49**, 299-312 (2010).

[8] Aubrey, M. L., *et al.* Electron delocalization and charge mobility as a function of reduction in a metal–organic framework. *Nat. Mater.* **17**, 625-632 (2018).

[9] Narayan, T. C., Miyakai, T., Seki, S., Dincă, M. High Charge Mobility in a Tetrathiafulvalene-Based Microporous Metal–Organic Framework. *J. Am. Chem. Soc.* **134**, 12932-12935 (2012).

[10] Sun, L., Miyakai, T., Seki, S., Dincă, M. Mn2(2,5-disulfhydrylbenzene-1,4-dicarboxylate): A Microporous Metal–Organic Framework with Infinite $(-Mn-S-)_{\infty}$ Chains and High Intrinsic Charge Mobility. *J. Am. Chem. Soc.* **135**, 8185-8188 (2013).

[11] Panda, T., Banerjee, R. High Charge Carrier Mobility in Two Dimensional Indium (III) Isophthalic Acid Based Frameworks. *Proc. Natl. Acad. Sci. India A* **84**, 331-336 (2014).